LAB ON A CHIP

A polymer-based microfluidic device for immunosensing biochips

Jong Soo Ko,*[ab] Hyun C. Yoon,*[ac] Haesik Yang,[a] Hyeon-Bong Pyo,[a] Kwang Hyo Chung,[a] Sung Jin Kim[a] and Youn Tae Kim[a]

[a] *BioMEMS Group, Basic Research Laboratory, ETRI, Daejeon 305600, Korea*
[b] *Department of Mechanical Engineering, Pusan National University, Pusan 609735, Korea. E-mail: mems@pnu.edu*
[c] *Division of Chemical Engineering & Biotechnology, Ajou University, Suwon 442749, Korea*

Received 14th February 2003, Accepted 25th March 2003
First published as an Advance Article on the web 30th April 2003

This paper describes the design, fabrication, and test of a PDMS/PMMA-laminated microfluidic device for an immunosensing biochip. A poly(dimethyl siloxane) (PDMS) top substrate molded by polymer casting and a poly(methyl methacrylate) (PMMA) bottom substrate fabricated by hot embossing are bonded with pressure and hermetically sealed. Two inlet ports and an air vent are opened through the PDMS top substrate, while gold electrodes for electrochemical biosensing are patterned onto the PMMA bottom substrate. The analyte sample is loaded from the sample inlet port to the detection chamber by capillary force, without any external intervening forces. For this and to control the time duration of sample fluid in each compartment of the device, including the inlet port, diffusion barrier, reaction chamber, flow-delay neck, and detection chamber, the fluid conduit has been designed with various geometries of channel width, depth, and shape. Especially, the fluid path has been designed so that the sample flow naturally stops after filling the detection chamber to allow sufficient time for biochemical reaction and subsequent washing steps. As model immunosensing tests for the microfluidic device, functionalizations of ferritin and biotin to the sensing surfaces on gold electrodes and their biospecific interactions with antiferritin antiserum and streptavidin have been investigated. An electrochemical detection method for immunosensing by biocatalyzed precipitation has been developed and applied for signal registration. With the biochip, the whole immunosensing processes could be completed within 30 min.

Introduction

Recently, developments in production methods of polymer-based microdevices have been in the limelight. Owing to the advent of microelectromechanical systems (MEMS) technology which grew out of integrated chip (IC) technology,[1–3] silicon has been widely used as a base material for microdevices. The key advantage of MEMS technology is that it allows sensing and actuation structures as well as driving circuits to be equipped on a single silicon wafer.[4,5] However, due to the high costs of material and fabrication, silicon is no longer competitive in comparison to polymers in markets for single-use microdevices.

Due to the rapid expansion of the microfluidics-based biochip market, including protein chips and DNA chips, many researchers have sought cost effective materials and fabrication methods.[6–9] In addition, market demand encourages the development of equipment for polymer microfabrication, leading to the successful development of several fabrication methods including casting,[10,11] embossing,[12,13] and injection molding.[14,15] Even nanometre-level structures can readily be realized through polymer casting or hot embossing methods.[8,12] It is now believed that polymers represent one of the most promising materials in the field of bioMEMS development. (BioMEMS refers to the use of MEMS based microdevices in biological applications).

Microfluidic components, including micropumps and microvalves, are generally required to control the fluid flow in MEMS. However, active microcomponents with moving parts are not easily integrated into polymer-based microfluidic devices due to the high fabrication costs and technical difficulties. In recent years, researchers have sought passive pumping and fluid-stopping components that could be substituted for the active microfluidic components.[16,17] As alternatives for controlling fluid flow without intervening moving parts, electrophoretic, electroosmotic, and capillary flows have been discussed. Electrophoretic and electroosmotic flows, which are driven by electrohydrodynamic phenomena,[18,19] generally induce the movement of very small volumes of liquid at a high driving voltage, resulting in difficulties in application for handheld or portable diagnostic systems. Therefore, microfluidic devices using these two methods have been utilized in bench-top equipment for DNA analysis, which involves ultra small liquid volumes and needs accurate flow rates. In contrast, capillary flow is naturally induced by surface tension between capillary surfaces and the liquid (so-called capillary force),[20] thus it doesn't need an additional power supply to induce the liquid flow. Furthermore, capillary flow is able to move non-conducting fluids as well as large liquid volumes compared with electrophoretic or electroosmotic flows. These aspects of capillary flow are advantageous in applications for handheld or portable diagnostic systems. In capillary flow, fluid flow can be controlled passively by the chemical modifications of surfaces and the geometrical changes in capillaries. Through surface modifications,[21–23] the surfaces of capillary tubes can be easily converted from hydrophilic to hydrophobic or *vice versa*. Hydrophobic surfaces that reduce capillarity stop the fluid flow, while hydrophilic surfaces that enhance capillarity induce the capillary flow. This means that the fluid flow in a capillary can be simply controlled by the appropriate combination of hydrophilic and hydrophobic surfaces. The geometrical change in a capillary, *i.e.* gradual or sudden expansion, is also a good method of fluid control. A sudden expansion stops the fluid flow, while a gradual expansion increases the flux by pressure

 DOI: 10.1039/b301794j

recovery. By utilizing a sudden expansion, the fluid flow can even be stopped in a capillary with a hydrophilic surface, without additional surface modifications.

In this study, we have developed and investigated a polymer-based microfluidic device for an immunosensing biochip, which would be directly adaptable for handheld diagnostic systems.[24–26] We have exploited the surface hydrophilicity and the conduit geometry to control the capillarity of a microfluid conduit as well as the flow of biofluids. As a model system for immunosensing with the fabricated device, we have investigated the functionalization of ferritin and biotin to the sensing monolayer and their biospecific interactions with the antiferritin antiserum and streptavidin samples. We have developed signal generation strategies for immunosensors, which transduce biospecific affinity reactions into electrochemical signals.[27–29] The voltammetric method, tracking the precipitation of insoluble products onto the sensing surface and subsequent decrement in the electrode area, is chosen for signal registration in this study.[29] Precipitation of insolubilities is induced by the biocatalytic reaction of enzymes, which were labeled to the biospecifically-attached antibody or streptavidin molecules.[30,31] This paper presents performance evaluations of the fabricated microfluidic device driven by capillary force and demonstrates its applicability as an immunosensing biochip. Details are reported herein.

Concept

The microfluidic device is comprised of a PDMS top substrate and a PMMA bottom substrate, as shown in Fig. 1A and 1B. The PDMS top substrate has two inlet ports and an air vent. The PMMA bottom substrate has gold electrodes and electric contacts patterned on it. They are bonded together by pressure, as shown in Fig. 1C. The analyte sample is loaded from the sample inlet port to the detection chamber by capillary force, without any intervening driving forces. Generally, the capillary force is too strong when the capillary is equipped with a hydrophilic surface and constant channel geometry (cross-sectional area), resulting in the sample fluid passing through the whole fluid conduit within several seconds. On the other hand, it is well known that an irregular fluid path increases the drag force so that the flow velocity is decreased. As an extreme case, a sudden expansion in a channel stops the fluid flow. In this study, to decrease the flow velocity and to control the time duration of sample fluid in each compartment of the device, including the inlet port, diffusion barrier, reaction chamber, flow-delay neck, and the detection chamber, we adopted substrate materials with relatively weak hydrophilic surfaces as well as modifying the fluid conduit with various channel lengths, cross-sectional areas, and shapes. The fluid path was designed so that the sample flow stops after the detection chamber has been filled, in order to allow sufficient time for biochemical reaction and subsequent washing step. The optimized dimension of each compartment was acquired through experimental results from numerous microfluidic test specimens with different channel and chamber sizes.

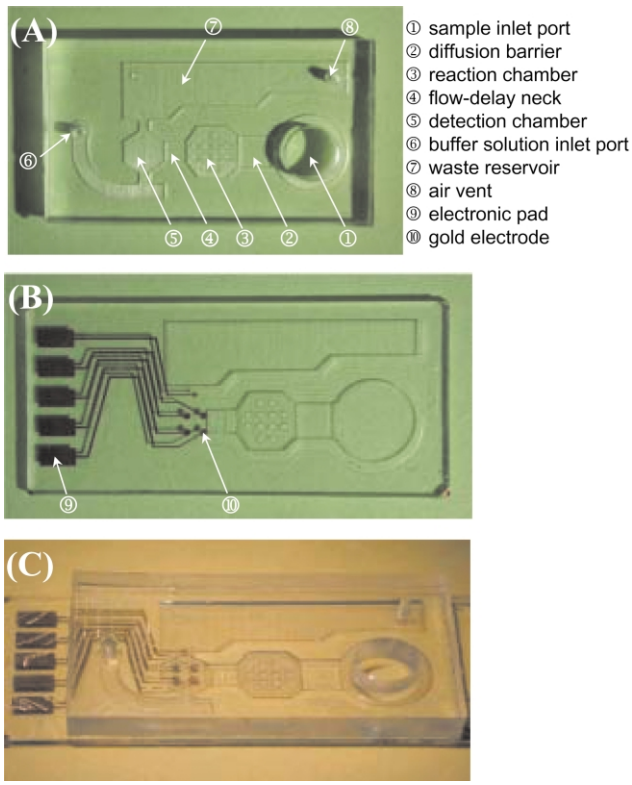

Fig. 1 Photographs of the fabricated polymer microfluidic device. (A) PDMS top substrate, (B) PMMA bottom substrate, and (C) the packaged device. Denotations: 1, sample inlet port, 2, diffusion barrier, 3, reaction chamber, 4, flow-delay neck, 5, detection chamber, 6, buffer solution inlet port, 7, waste reservoir, 8, air vent, 9, electronic pad, and 10, gold electrode.

The diffusion barrier, which is located between the inlet port and reaction chamber, reduces the cross sectional area of the channel, so that it separates the freshly applied sample in the sample inlet port from the reacted sample in the reaction chamber. Thus it minimizes the inter-diffusion between two samples. The secondary antibody, which will react with the applied sample, is evenly spread onto the surface of the reaction chamber before encapsulation. While the secondary antibody solution is being dried in the reaction chamber, the micro-hills constructed in the chamber prevent the solution from gathering at the corners of the reaction chamber, facilitating uniform spreading of secondary antibodies. The flow-delay neck is designed to retard the flow drastically, so that it permits sufficient reaction time between the analyte sample (primary antibody to target molecule) and secondary antibodies in the reaction chamber. Flow retardation is achieved by reducing the channel width and depth of the flow-delay neck. After passing the flow-delay neck, the reacted sample fills the detection chamber. Then the flow stops due to the sudden expansion at the left and right sides of the detection chamber.

While staying in the detection chamber, the reacted analyte complex (antibody conjugates) binds biospecifically to the antigen or ligand moieties anchored to the gold electrode surfaces. For the catalytic reaction of enzymes and the electrochemical detection, the sample remnant and the non-specifically bound byproducts in the detection chamber are washed and replaced with a buffer solution, which is injected through the buffer solution inlet port by an external syringe pump. After that, the signal generation reaction and the electrochemical detection step proceed.

Experimental

Materials

Poly(dimethylsiloxane) and its curing agent were purchased from Dow Corning (PDMS, SYLGARD® 184), and PMMA was obtained from LG (PMMA IF870, Korea). Amine-terminated poly(amidoamine) dendrimer (G4) is manufactured by Dendritech and was purchased from Aldrich. Ferrocene methanol was purchased from Aldrich and used as received. 3,3-Dithiopropionic acid bis-*N*-hydroxysulfosuccinimide ester (DTSSP) and EZ Link biotin-poly(ethylene oxide)-amine were obtained from Pierce and used as received. 3,3-Dithiopropionic acid bis-*N*-hydroxysuccinimide ester (DTSP), biotinyl-amido-caproic acid *N*-hydroxysulfosuccinimide ester (sulfo-NHS-

biotin), and 4-chloro-1-naphthol (4-CN) were purchased from Sigma. Horse spleen ferritin (cationized, functionalized with dimethylpropanediamine), anti-horse ferritin rabbit whole antiserum, anti-rabbit IgG–horseradish peroxidase (HRP) conjugate (developed in goats), and streptavidin-HRP conjugate were from Sigma and used without further purification. All other materials used were of the highest quality available and purchased from regular sources. For solutions, doubly distilled and deionized water with a specific resistance over 18 MΩ cm was used throughout the study.

Fabrication of the microfluidic device

The masters for replications of the PDMS and PMMA substrates were made of aluminium and special-use stainless (SUS) steel, as shown in Fig. 2A and 2B, respectively. Computer numerical control (CNC) machining was used to fabricate the masters. Even though it is difficult to get smoothly machined surfaces from SUS compared to aluminium, SUS was chosen because it has good mechanical properties so that the microstructures in the master do not deform after the hot embossing process with high temperatures and pressures. The PDMS top substrate was molded by polymer casting, and the PMMA bottom substrate, onto which gold electrodes were patterned, was fabricated by hot embossing. An 8 : 1 (v/v) mixture of PDMS prepolymer with its curing agent was poured onto the aluminium master and cured at 100 °C for 15 min in a vacuum oven. Then, the solidified PDMS substrate was peeled off from the aluminium master. Three aluminium pillars were fixed onto each section of the aluminium master and a 3 mm high aluminium fence was hermetically surrounded along its edge, as shown in Fig. 2A. As a result, a 3 mm thick PDMS top substrate with three holes could be obtained without any additional punching or cutting as in Fig. 1A. For the bottom substrate, a 1 mm thick PMMA sheet was embossed with the SUS master at 130 °C and pressing force of 5 kN. The vicat softening temperature of the PMMA, *i.e.* the temperature at which the specimen is penetrated 1 mm deep by a flat-end needle, was 95 °C. Cr (20 nm) and Au (200 nm) layers were then consecutively deposited onto the embossed PMMA substrate by an E-beam evaporator, as shown in Fig. 1B. Prior to the Cr/Au deposition, a 100 μm thick shadow mask (Fig. 2C), which was laser cut as the pattern of gold electrodes, was aligned and clamped on the embossed PMMA substrate. Separately prepared PDMS and PMMA substrates were then bonded with pressure at room temperature and hermetically sealed. The freshly prepared PDMS substrate exhibited satisfactory bonding strength to the PMMA substrate, and the plasma treatment was not necessary in this case. Fig. 1C shows the fabricated microfluidic device with the size of 35 × 17 × 4 mm^3.

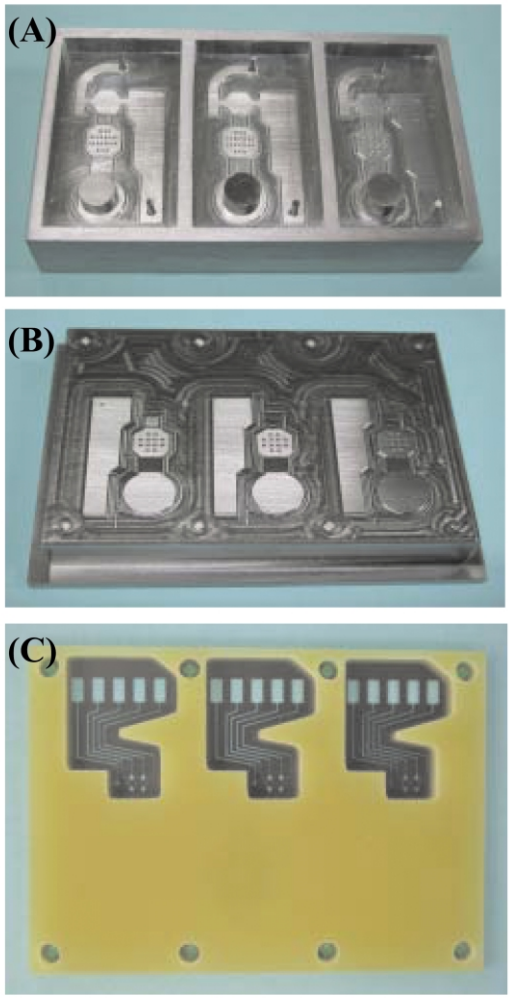

Fig. 2 Photographs of two metal masters and a shadow mask used for the biochip fabrication. Three polymer microfluidic devices are obtained from one batch fabrication. (A) Aluminium master for PDMS top substrate replica. (B) SUS master for PMMA bottom substrate replica. (C) Stainless steel shadow mask for patterning of the Cr/Au electrodes.

Construction of the affinity sensing surface on gold

A schematic representation of the chemically modified and biofunctionalized electrode surface and the signal generation reaction are summarized in Fig. 3. As the first step, a DTSSP self-assembled monolayer (SAM) was constructed on the freshly evaporated gold electrodes, which were patterned on the PMMA bottom substrate, to render the surface amine-reactive. The DTSSP SAM was prepared by spotting 1 μL aliquots of 5 mM DTSSP in water on each electrodes and incubating for 1 h. After DTSSP monolayer formation, electrode surfaces were modified with antigen (ferritin) or ligand (biotin) molecules. A diluted solution of ferritin or biotin-PEO-amine in a phosphate buffered saline (PBS, pH 7.4, 10 mM phosphate, 2.7 mM KCl, and 138 mM NaCl containing 0.05% (v/v) Tween 20) was spotted and reacted (2 h) with the succinimidyl ester-activated surfaces. Then, the modified surfaces were rinsed and stored in PBS for further biospecific affinity reactions.

For the fabrication of dendrimer-assisted biosensing surface as a comparison test, a dendrimer monolayer formation step was added. After DTSP monolayer formation in place of the DTSSP SAM and rinsing steps with DMSO and ethanol, the electrode surface was incubated with G4 poly(amidoamine) dendrimer solution. A diluted ethanolic solution of dendrimer (1% w/w) was reacted (2 h) with the prepared DTSP-activated surfaces. Then, the dendrimer-modified surfaces were further underwent the biofunctionalization steps.

Affinity sensing procedures

Biospecific protein binding on the constructed affinity sensing surfaces was performed with model analyte samples including antiferritin antiserum and streptavidin. All the protein samples are in the form of horseradish peroxidase (HRP) conjugates for the enzyme-catalyzed signal generation reaction.

After the biochip assembly, biospecific affinity reactions were performed with target protein samples. For the streptavidin affinity reaction (Fig. 3A), lyophilisate streptavidin-HRP was dissolved into PBST to the concentration of 20 μg protein mL^{-1} and loaded from the sample inlet port to the electrode in the detection chamber at room temperature. The biospecific affinity reaction between the biotin functionality on electrodes surfaces and the streptavidin-HRP was performed for 15 min. For the ferritin immunosensing (Fig. 3B), aliquots of ferritin

antiserum (100 μL) of predetermined whole protein concentration (100 μg mL^{-1}) were prepared in PBST and used. Ferritin immunosensing with the biochip was conducted in two ways, the stepwise reaction mode and the whole processes on a chip mode. In the stepwise reaction mode, the process for the complex formation of primary-IgG in the antiserum with secondary antibody-HRP conjugate was performed outside the immunosensing biochip to extend the time duration of complex formation, alleviating the effect from limited affinity reaction yield. After mixing and reacting the antiserum with the secondary antibody-HRP for 1 h, the sample was loaded to the biochip, and the biospecific recognition between the electrode surface-immobilized antigens and the antibody complex was performed for 15 min. In the other mode, the whole processes were conducted on a single chip, consisting of the antibody complex formation step in the reaction chamber while the flow was retarded at the flow-delay neck (8 min) and the biospecific recognition reaction at the electrode surface (15 min).

Following the affinity recognition reaction, the antibody- or streptavidin-associated surfaces were subjected to the signal generation/measurement step,[29] after rinsing and loading the signalling solution from the second inlet port on the biochip. For the signal generation, enzyme-catalyzed precipitate formation reaction was performed, and the reaction couple of HRP with 4-chloro-1-naphthol (4-CN) was used. Ethanolic 4-CN was initially prepared to the concentration of 50 mM. Fifty microlitre aliquots of prepared 4-CN and 30% hydrogen peroxide were added to 1 mL of PBS solution briefly before the precipitation reaction. Then, the electrode surface was subjected to the signal generation reaction by incubating with the analysis mixture for 10 min.

Instrumentation

Cyclic voltammetric measurements were carried out with a potentiostat/galvanostat (model 660A, CHI instruments) connected to a laptop computer. A standard three-electrode configuration with gold thin-film working and auxiliary electrodes and an external Ag/AgCl (diameter 6 mm, 3 M NaCl, BAS) reference electrode was used throughout the study. After biochip assembly, an Ag/AgCl reference electrode was placed in the opening of sample inlet port and the voltammetric measurements were conducted. Cyclic voltammetric measurements were performed either in 0.1 M phosphate buffer, pH 7.0, as the background electrolyte or in a buffer solution containing 0.1 mM ferrocene methanol for signal registration. All experiments were performed at room temperature under ambient condition.

Results and discussion

Flow characterization

Keeping the different flow velocities in each channel and chamber is the key concern in this microfluidic device. Utilizing a digital camera and a camcorder, the stopping, flowing, and mixing of the fluid in each compartment as well as the partial delamination between the PDMS and PMMA substrates at the pressure-built-up points were observed and characterized. Fig. 4 shows the time-lapse images of the sample flow with red dye dissolved in the sample analyte. After filling the analyte sample inlet port (7 mm diameter and 600 μm depth), the freshly applied sample (100 μl) flowed in the diffusion barrier for 2 min by capillary force. To minimize the inter-diffusion between the freshly applied sample and reacted sample in the reaction chamber, the channel cross sectional area of diffusion barrier was narrowed to 3 mm in width and 200 μm in depth. Immediately after passing the diffusion barrier, the analyte sample readily wetted the reaction chamber surface (Fig. 4A), where the secondary antibody was coated before encapsulation. The measured contact angle of the surface coated with

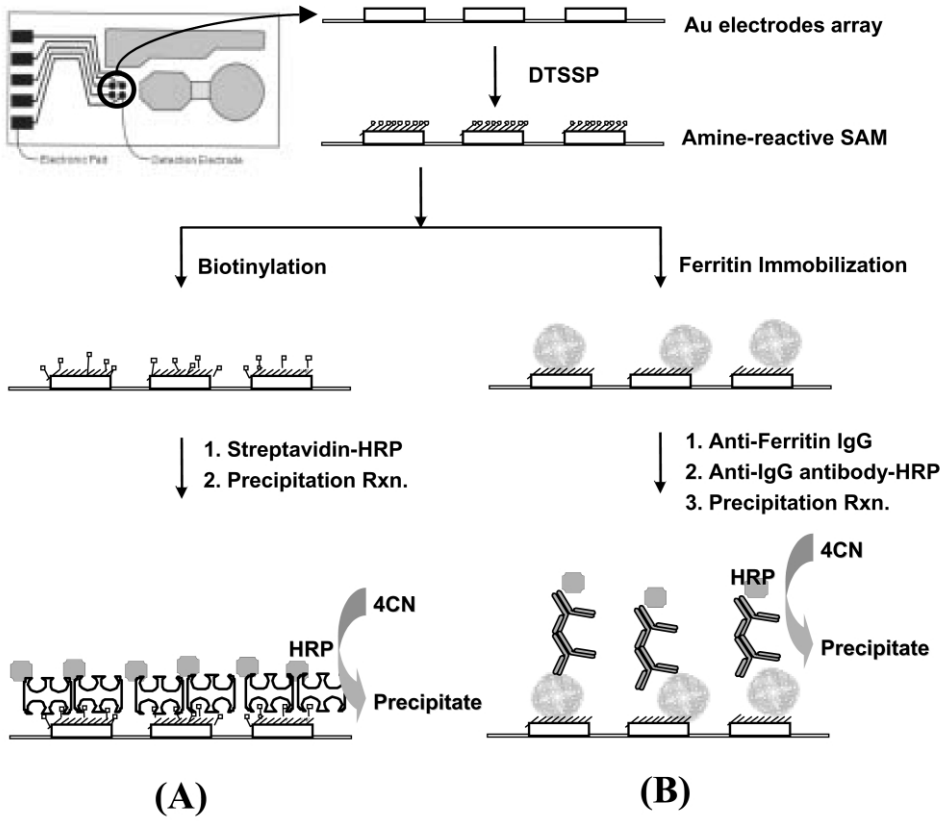

Fig. 3 Schematic representation of the procedure employed for the affinity surface construction and the proposed operational principle of the immunosensing biochips. (A) Streptavidin/biotin-functionalized recognition surface. (B) Antiferritin-antiserum/ferritin antigen-immobilized surface. The dimensions of the components are not drawn to scale for simplicity.

secondary antibody was about 30°, showing that the surface was rendered hydrophilic by protein coating. While the secondary antibody solution is drying, the micro-hills fabricated in the reaction chamber prevent the solution from gathering at the corners of the chamber, thereby facilitating uniform distribution of dried secondary antibody molecules. The flow-delay neck retards the flow (Fig. 4B), so that it permits *ca.* 8 min for the reaction between the analyte sample and secondary antibody in the reaction chamber. We achieved this flow retardation in two ways: by narrowing the conduit to a 2 mm width and 200 μm depth, and by duplicating the drag forces at the diffusion barrier and the reaction chamber. After passing the flow-delay neck, the reacted analyte sample filled the detection chamber, and then the flow stopped due to the significant difference in the capillarity by sudden expansions of 180° at the openings of the detection chamber (Fig. 4C). Menisci at the flow fronts of the two openings clearly show the static force equilibrium between the capillary and flow resisting forces by sudden expansion. The reacted analyte sample remained in the detection chamber for 15 min, so that the reacted analyte conjugates bound biospecifically to the antigen moieties anchored to the gold electrode surface. The detection chamber was successively washed and replaced with solutions by an external syringe pump (flow rate: 2 ml min^{-1}) for subsequent biosensor signal generation and electrochemical detection steps (Fig. 4D). The washed solutions were collected in the waste reservoir. The whole process, including affinity reactions, signaling, and electrochemical detection was completed within 30 min.

It was empirically found that the freshly prepared PDMS substrates offered stronger bonding to the PMMA substrate, comparing to the previously prepared and stored ones. Significant delamination was not observed at any laminated regions because very low fluid pressure was applied in this microfluidic device. It is well known that polymer casting and hot embossing processes are adequate for replication of nanostructures on surfaces. It means that the fabricated PDMS and PMMA substrates have been thoroughly replicated from the masters. There are two key issues in the polymer replication in microscale: how to enhance the accuracy of the microstructures of the original masters and how to minimize the roughness of their micromachined surfaces. Electroplated nickel masters and deep-etched silicon masters fabricated by MEMS technology can be good means to satisfy these requirements.[32] In our study, we have adopted chemical–mechanical-polishing (CMP) process to get smooth surfaces of the metal masters to achieve good bonding results.

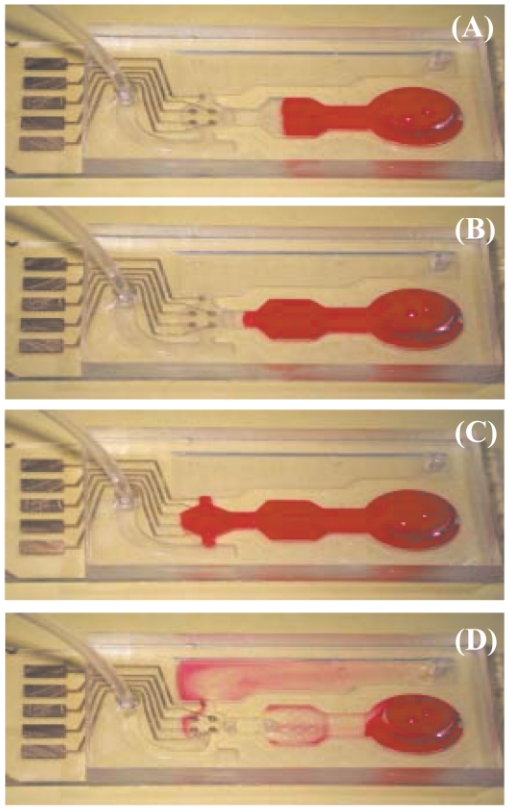

Fig. 4 Captured images for visualization of the flow sequence. (A) The analyte sample injected from the analyte inlet port is flowing in the reaction chamber. (B) The flow is passing through the flow-delay neck. (C) The analyte sample filled the detection chamber and the flow stopped. (D) The washing solution injected from the buffer solution inlet port is flowing in the detection chamber and the waste reservoir is being filled.

Electrochemical immunoassay using the fabricated biochips

Immunosensing tests with the fabricated polymer-based microfluidic devices were conducted as follows. The affinity sensing surfaces were made by spotting antigens or ligand biomolecules onto the electrodes, which were fabricated on the PMMA bottom substrate as a 2 × 2 array format. The main focuses of the development of an immunosensing biochip reside in (1) the method of biofunctionalization that is compatible with Au/PMMA surface, (2) the minimization of signal interference (crosstalk) between neighboring electrodes constituting the array, and (3) the efficient signalling of the immunoassay with the whole antiserum sample at the single biochip, not with the pre-purified antibody samples.

First, for the functionalization of antigen and ligand molecules at the array electrodes and further immunosensing reactions, a platform surface that represents compatibility with the PMMA polymer substrate was necessary. For the objective, a self-assembled monolayer of alkanethiolate and a dendrimer-activated surface monolayer, representing active functionalities for protein immobilization, were made on the patterned gold electrodes. The detailed steps for the fabrication of reactive surfaces are as shown in Fig. 3, and the method is applicable both to the protein antigen immobilization and the ligand (biotin) functionalization. A self-assembled monolayer of DTSSP, which represents *N*-hydroxysulfosuccinimide functional groups, was prepared by spotting aqueous DTSSP solution to the gold electrode surface. The DTSSP, a sulfonated and ionizable derivative of DTSP, is soluble in the aqueous solution and is useful, since the polar aqueous solution is not dispersed on the hydrophobic Au/PMMA surface, which is beneficial for the spotting of solutions on a small scale on hydrophobic surfaces. After SAM formation, the *N*-hydroxy(sulfo)succinimide group is exposed at the surface, which is accessible to the amine functional groups from proteins and ligands. By the same method, poly(amidoamine) dendrimer molecules could also be immobilized on the sensor surface for further biofunctionalization reactions as well as the direct immobilization of biomolecules containing surface amine groups. The dendrimer-modified portion of the electrode surface works as the base platform for further ligand functionalization and biospecific interactions with target proteins.

The electrochemical signalling system with the prepared affinity-sensing surface was constructed for the evaluation of the biospecific interaction between immobilized antigen and ligand molecules with the reaction couple in biofluids. As the model reactions, biotin/streptavidin and ferritin/antiferritin-antiserum reaction couples were used. We chose the biotinyl ligand group because there exist further applicational capabilities incorporating biotinylated biomolecules, *e.g.* nucleic acids, lectins, and biopolymers. Ferritin was adopted because it contains multiple binding sites for antiferritin antibody recognition (multivalency), enabling the reaction under less strict conditions in terms of molecular orientation, which is usually crucial for affinity recognition reactions at surfaces.

Fig. 5 shows the electrochemical signaling results for the ferritin/antiferritin-antiserum affinity sensing with the recognition surfaces of dendrimer-assisted SAM (A) and DTSSP SAM (B). Ferritin immunosensing with the biochip was conducted in the stepwise reaction mode, minimizing the effect from the limited reaction yield of antibody complex formation (see Experimental Section). The cyclic voltammetric method, tracking the precipitation of insoluble products onto the sensing surface and subsequent decrement in the electrode area, was chosen for signal registration. Precipitation of insolubilities was induced by the catalytic reaction of HRP, which were labeled to the biospecifically-attached secondary antibody molecules for antiferritin antibody. The methodology related to biological reaction and electrochemical detection was established previously and is described in detail elsewhere.[29]

The two surfaces were prepared and compared in terms of density of biomolecular functionalization and sensing efficiency. Dendrimer-assisted SAM had been found advantageous for biofunctionalization on gold and glass surfaces from the molecular characteristics of dendrimers.[33–35] However, in the present work, the dendrimer-assisted SAM was found not compatible with PMMA polymer substrate because dendrimer molecules readily adsorb on to the hydrophobic PMMA surface and form aggregates. As in Fig. 5A, the electrode based on dendrimer-assisted SAM exhibited increased background charging current and small signal change after the biocatalyzed precipitation reaction. With the surface based on the DTSSP SAM (Fig. 5B), on the other hand, the signal change after biospecific affinity reaction and precipitation was distinct, confirming the electrode responded well. The cyclic voltammograms presented in Fig. 5 were registered from the tests after optimization experiments for the affinity-surface fabrication and signaling reaction had completed. From this result, the decrements in the active electrode area could be interpreted as the extent of biocatalyzed reaction as well as the surface density of biospecifically attached biomolecules. Furthermore, DTSSP is soluble in water, and the aqueous solution could be easily deposited on to the hydrophobic Au/PMMA surface by simple spotting without dispersion.

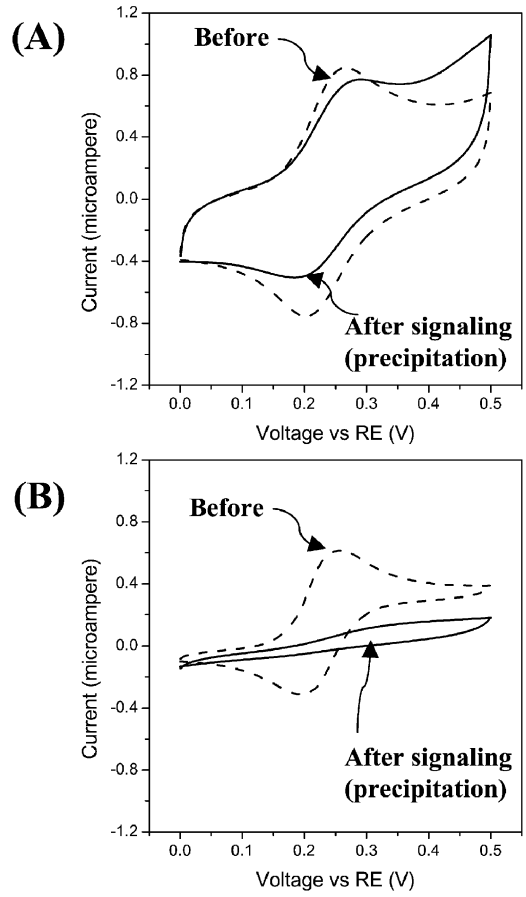

Fig. 5 Cyclic voltammograms of affinity electrodes for ferritin at different surface construction platforms: (A) Poly(amidoamine) dendrimer (G4)-assisted SAM. (B) DTSSP SAM. Each panel contains voltammograms registered before (dashed curves) and after the signaling step (solid curves). Cyclic voltammetric measurements were performed in 0.1 M phosphate buffer, pH 7.0 containing 0.1 mM ferrocene methanol as an electroactive signal tracer. Voltage sweep rate was 50 mV s^{-1}.

With this advantage, site-by-site immobilization of different target analytes on the 2 × 2 array electrodes was attempted to evaluate the effect of signal interference (crosstalk) between the neighboring electrodes. As shown in Fig. 6, the site-by-site immobilizations of antigen (ferritin) and ligand group (biotin) on electrode array were conducted. Of the 2 × 2 array, two electrodes were modified with ferritin (electrode b) and biotin (electrode c) functional groups. Another site (electrode a) was modified with only DTSSP SAM, and the level of nonspecific protein adsorption was determined after the active ester groups

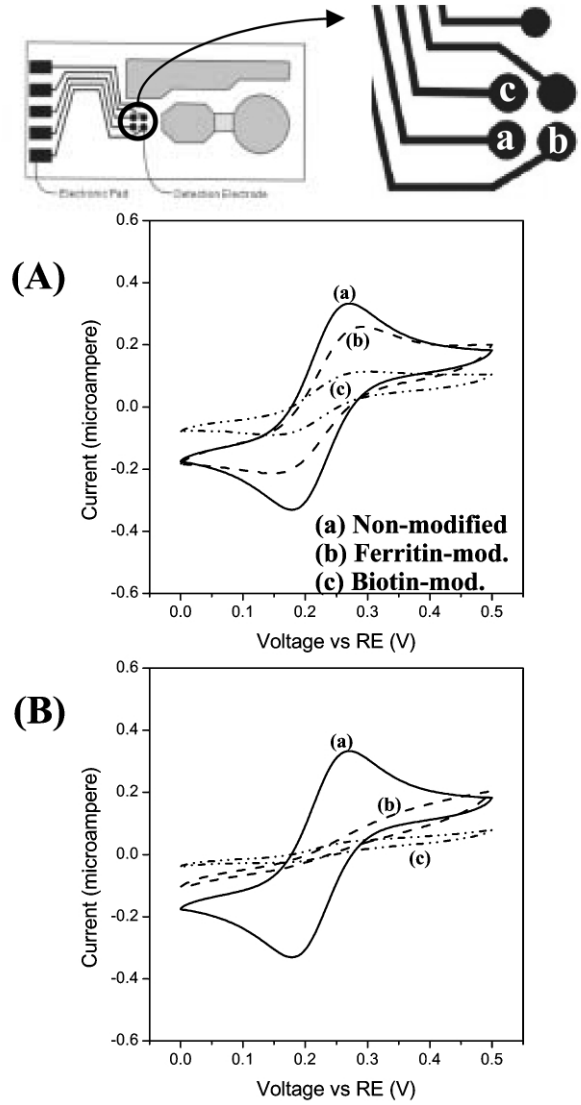

Fig. 6 Cyclic voltammograms of affinity electrodes constituting the immunosensing biochip for the evaluation of the effect from signal crosstalk between neighboring electrodes: (A) cyclic voltammetric result from the first affinity reaction with streptavidin-HRP and (B) cyclic voltammetric result from the second immunosensing reaction with antiferritin-IgG/secondary IgG-HRP. Each panel contains voltammograms from electrodes constituting the 2 × 2 array: (a) non-modified electrode (control), (b) ferritin-immobilized electrode, and (c) biotin-functionalized electrode. Cyclic voltammetric measurements were performed in 0.1 M phosphate buffer, pH 7.0 containing 0.1 mM ferrocene methanol as an electroactive signal tracer. Voltage sweep rate was 50 mV s^{-1}.

were quenched. The tests were conducted by sequential reaction by streptavidin-HRP and antiferritin-IgG/secondary IgG-HRP complex to the same device. The first immunosensing reaction was performed with the streptavidin-HRP (Fig. 6A). After the injection of the streptavidin-HRP to the analyte inlet port, the affinity reaction and signaling steps by the biocatalyzed precipitation were conducted. Fig. 6A shows the resulting cyclic voltammograms after the signaling reaction. Trace (a) is for the non-modified electrode, (b) is for the ferritin-functionalized surface, and (c) is for the biotin-functionalized surface. From the result, trace (c) exhibited distinctly suppressed peak currents, showing that the loaded streptavidin-HPR biospecifically attached to the biotinylated surface and the precipitation reaction was efficiently induced. In comparison, electrodes (a) and (b) showed little or no retardation of the ferrocene peak currents (traces a, b in Fig. 6A), showing that the electrodes are not contaminated by the precipitate formed from the adjacent electrode (c). The difference between the voltammograms (a) and (b) is probably from the immobilized ferritin molecules themselves, which marginally block the electrode surface. The second immunosensing reaction on the same biochip was performed with the antiferritin-IgG/secondary antibody-HRP complex. After the injection of the sample from the analyte inlet port, the same affinity reaction and signaling steps were conducted. Fig. 6B shows the cyclic voltammograms after the second signaling reaction. Trace (b) is for the ferritin-modified electrode, which responded well from the result. For the biotin-functionalized electrode (c), however, a voltammogram of more flattened form was registered. This result is from the fact that the preadsorbed streptavidin-HRP in the first reaction step still maintains the reactivity and the biocatalyzed precipitation reaction proceeds under the same reaction condition. From the experiments, it was found that the signal interference between the neighboring electrodes is not significant and the array format biosensing would be feasible.

It should be noted that the portion of electrolyte in which biospecific affinity interaction and signal generation reaction occur is restricted to within several nanometres from the functionalized sensing monolayer. The estimated thickness of the reaction layer where precipitation reaction would happen is about 10–20 nm based on the molecular sizes of antibody and HRP molecules. From this, it is assumed that the precipitates that were produced during the biocatalytic reaction with the associated (labeled) HRP would readily adsorb on to the electrode surface, excluding the possibility of lateral movement and contamination of the adjacent electrode in case of microarray-type biosensors. In other words, the shortened path of the insoluble enzyme product facilitates the precipitation and insulating film formation, supporting rapid and efficient sensor signaling. Thus, this signaling format would benefit from the concept of parallel detection with microarray biosensors.

The affinity reaction for ferritin immunoassay is composed of two stepwise reactions, (1) the complex formation of primary-IgG with secondary antibody-HRP conjugate and (2) the biospecific recognition between the electrode surface-immobilized antigens with the antibody complex. In the final design of the immunosensing biochip, the first step of antibody complex formation takes place in the reaction chamber. However, in the experiment, the step of antibody complex formation was performed outside the immunosensing biochip to extend the time duration of complex formation. When the entire reactions are performed on the biochip, the affinity reactions are restricted by the limited reaction time and the continuous capillary flow. From this viewpoint, both the cases of the stepwise reaction and the whole processes on an immunosensing biochip were conducted and compared, as in Fig. 7. For the stepwise and separated reaction (Fig. 7A), the complex formation of primary-IgG and secondary antibody-HRP was performed for 1 h, and the biospecific recognition between the electrode surface-immobilized antigens with the antibody complex was performed for 15 min. From the resulting entirely suppressed voltammogram (A), it was found that the immunosensor responded well, confirming that the reaction time durations were sufficient and the desired affinity reactions took place efficiently. In case of Fig. 7B, when the whole processes are performed on a single biochip, the step of antibody complex formation was conducted in the reaction chamber for 8 min while the flow was retarded at the flow-delay neck, and the biospecific recognition reaction at the electrode surface was conducted for 15 min. From the result (voltammogram B), the feasibility of the whole process on a biochip mode for ferritin immunosensing was evident, but the signal efficiency and reaction yield did not reach the final satisfactory level. Studies on the reaction optimization are under progress in our group.

Conclusions

In this paper, we have introduced a PDMS/PMMA-laminated microfluidic device working on capillary flow and have demonstrated the applicability of the technology to the electrochemical immunosensing biochip. The result showed that the fluid flow could be precisely yet passively controlled through surface modifications and geometrical changes of the capillary, and the proposed electrochemical immunoassay method represented a simple method of integrating detection into the microfluidic device. Therefore, the proposed microfluidic device provides a good route for realizing disposable biochips for portable diagnostic systems. Diagnostic systems adopting the proposed microfluidic device and electrochemical

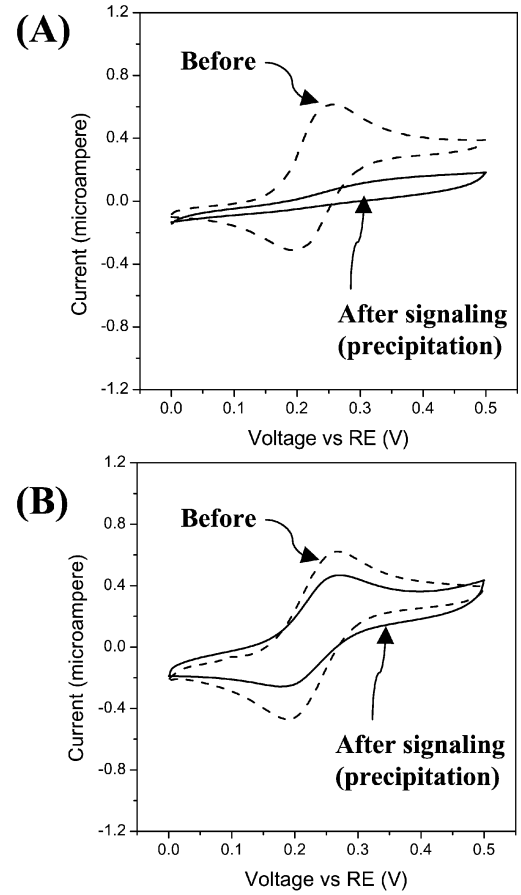

Fig. 7 Electrochemical signaling from the ferritin immunosensing biochip at different operational modes: (A) Stepwise and separated reaction. (B) Whole processes on a biochip. Each panel contains voltammograms registered before (dashed curves) and after the signaling step (solid curves). Conditions for the electrochemical tests were the same as Fig. 5.

detection would be realized as small-sized, light-weight, and low-power systems.

Acknowledgements

The present work was financially supported by Grant-in-Aids for Scientific Research from the Ministry of Information and Communication, Korea.

References

1 K. E. Petersen, *IEEE Trans. Electron Devices*, 1978, **ED-25**, 1241–1249.
2 S. C. Terry, J. H. Jermann and J. B. Angell, *IEEE Trans. Electron. Devices*, 1979, **ED-26**, 1880–1886.
3 H. B. Chan, V. A. Aksyuk, R. N. Kleiman, D. J. Bishop and F. Capasso, *Science*, 2001, **291**, 1941–1944.
4 G. T. A. Kovacs, *Micromachined Transducers Sourcebook*, McGraw-Hill, New York, 1998.
5 J. S. Ko, M. L. Lee, D.-S. Lee, C. A. Choi and Y. T. Kim, *Appl. Phys. Lett.*, 2002, **81**, 547–549.
6 L. T. Romankiw, *Electrochim. Acta*, 1997, **42**, 2985–3005.
7 S. R. Quake and A. Scherer, *Science*, 2000, **290**, 1536–1539.
8 H. Becker and C. Gärtner, *Electrophoresis*, 2000, **21**, 12–26.
9 S. A. Soper, S. M. Ford, S. Qi, R. L. McCarley, K. Kelly and M. C. Murphy, *Anal. Chem.*, 2000, 643A–651A.
10 J. R. Anderson, D. T. Chiu, R. J. Jackman, O. Cherniavskaya, J. C. McDonald, H. Wu, S. H. Whitesides and G. M. Whitesides, *Anal. Chem.*, 2000, **72**, 3158–3164.
11 J. C. McDonald and G. M. Whitesides, *Acc. Chem. Res.*, 2002, **35**, 491–499.
12 S. Y. Chou, P. R. Krauss and P. J. Renstrom, *Appl. Phys. Lett.*, 1995, **67**, 3114–3116.
13 L. Martynova, L. E. Locascio, M. Gaitan, G. W. Kramer, R. G. Christensen and W. A. MacCrehan, *Anal. Chem.*, 1997, **69**, 4783–4789.
14 R. M. McCormick, R. J. Nelson, M. G. Alonso-Amigo, D. J. Benvegnu and H. H. Hooper, *Anal. Chem.*, 1997, **69**, 2626–2630.
15 A. Olsson, O. Larsson, J. Holm, L. Lundbladh, O. Öhman and G. Stemme, *Sens. Actuators A*, 1998, **64**, 63–68.
16 P. G. Wapner and W. P. Hoffman, *Sens. Actuators B*, 2000, **71**, 60–67.
17 H. Andersson, W. van der Wijngarrt, P. Griss, F. Niklaus, G. Stemme and P. G. Wapner, *Sens. Actuators B*, 2001, **75**, 136–141.
18 D. J. Harrison, K. Fluri, K. Seiler, Z. Fan, C. S. Effenhauser and A. Manz, *Science*, 1993, **261**, 895–897.
19 A. Manz, C. S. Effenhauser, N. Burggraf, D. J. Harrison, K. Seiler and K. J. Flurri, *J. Micromech. Microeng.*, 1994, **4**, 257–265.
20 F. M. White, *Fluid Mechanics*, McGraw Hill, New York, 5th edn., 2002.
21 E. Delamarche, A. Bernard, H. Schmid, B. Michel and H. Biebuyck, *Science*, 1997, **276**, 779–781.
22 P. Lam, K. J. Wynne and G. E. Wnek, *Langmuir*, 2002, **18**, 948–951.
23 S. Hu, X. Ren, M. Bachman, C. E. Sims, G. P. Li and N. Allbritton, *Anal. Chem.*, 2002, **74**, 4117–4123.
24 A. J. Tüdos, G. A. J. Besselink and R. B. M. Schasfoort, *Lab Chip*, 2001, **1**, 83–95.
25 D. R. Reyes, D. Iossifidis, P.-A. Auroux and A. Manz, *Anal. Chem.*, 2002, **74**, 2623–2636.
26 P.-A. Auroux, D. Iossifidis, D. R. Reyes and A. Manz, *Anal. Chem.*, 2002, **74**, 2637–2652.
27 H. C. Yoon, M.-Y. Hong and H.-S. Kim, *Anal. Biochem.*, 2000, **282**, 121–128.
28 H. C. Yoon, M.-Y. Hong and H.-S. Kim, *Langmuir*, 2001, **17**, 1234–1239.
29 H. C. Yoon, H. Yang and Y. T. Kim, *Analyst*, 2002, **127**, 1082–1087.
30 F. Patolsky, M. Zayats, E. Katz and I. Willner, *Anal. Chem.*, 1999, **71**, 3171–3180.
31 R. Jenison, S. Yang, A. Haeberli and B. Polisky, *Nature Biotech.*, 2001, **19**, 62–65.
32 J. Xu, L. Locascio, M. Gaitan and C. S. Lee, *Anal. Chem.*, 2000, **72**, 1930–1933.
33 D. C. Tully and J. M. J. Fréchet, *Chem. Commun.*, 2001, **14**, 1229–1239.
34 R. Benters, C. M. Niemeyer, D. Drutschmann, D. Blohm and D. Wöhrle, *Nucleic Acids Res.*, 2002, **30**, e10.
35 M.-Y. Hong, H. C. Yoon and H.-S. Kim, *Langmuir*, 2003, **19**, 416–421.